THE JOURNAL OF PHYSICAL CHEMISTRY C

Article

pubs.acs.org/JPCC

Near- and Far-Field Effects on the Plasmon Coupling in Gold Nanoparticle Arrays

Xiaoli Wang,[†,‡] Philippe Gogol,[§] Edmond Cambril,[∥] and Bruno Palpant*[,†]

[†]Ecole Centrale Paris, Laboratoire de Photonique Quantique et Moléculaire, CNRS UMR 8537, Ecole Normale Supérieure de Cachan, Grande Voie des Vignes, F-92295 Châtenay-Malabry cedex, France

[‡]Institut des NanoSciences de Paris, CNRS UMR 7588, Université Pierre et Marie Curie, 4 place Jussieu, F-75252 Paris cedex, France

[§]Institut d'Electronique Fondamentale, CNRS UMR 8622, Université Paris-Sud, F-91405 Orsay cedex, France

[∥]Laboratoire de Photonique et de Nanostructures, CNRS UPR20, Route de Nozay, F-91460 Marcoussis, France

ABSTRACT: Understanding the plasmon coupling between metal nanoparticles under light irradiation remains a challenging issue for optimizing plasmonic devices for chemical and biological sensing. Here, the optical properties of dense spatially ordered two-dimensional arrays of 50 nm gold nanoparticles are investigated in this aim. Microspectrophotometry experiments are carried out on square arrays and parallel chains, elaborated by electron beam lithography, having different periodicities ranging from 80 to 170 nm. The wavelength, width, and amplitude of the localized surface plasmon resonance (SPR) are quantitatively monitored as a function of both the incident light polarization and the interparticle distance. The experimental findings are then compared with calculations based on the discrete dipole approximation. They match remarkably well these numerical results, not only for the spectral location and the width of the SPR but also for the absolute value of the extinction cross section of the nanoparticles that is linked with the local field enhancement. The variation of the SPR band characteristics as a function of the periodicity of the arrays is investigated in terms of near-field and far-field coupling effects by discussing the topography of the field amplitude and phase in the arrays. Moreover, in order to highlight the influence of phase retardation and radiative effects on the plasmon coupling, the optical properties of equivalent arrays scaled by 1/10, which can be qualitatively described by electrostatic dipolar interactions, are also studied by numerical calculations. The discrepancies then observed between the two scales are interpreted. The contributions of the radiative and nonradiative dampings to the width and magnitude of the plasmon resonance are also investigated.

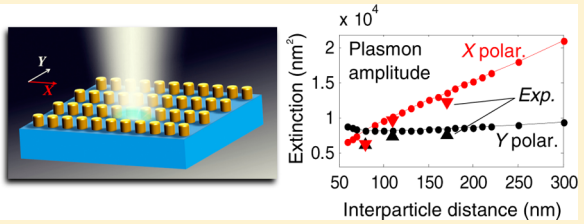

INTRODUCTION

Noble metals confined at the nanoscale exhibit the well-known localized surface plasmon resonance (SPR) associated with the enhancement of the local electromagnetic field in the particles. The plasmon resonance is very sensitive to the shape, size, and composition of the particles and surrounding medium, which may influence the spectral position, width, and amplitude of the resonant absorption. Besides, the interparticle coupling also plays an important role in the plasmon properties.[1−5] As a result, complex nanostructures with controllable dimensions such as nanorod assemblies or spatially ordered nanoparticle arrays have raised great interest in many applications such as surface enhanced Raman scattering (SERS),[6−8] biosensing,[9,10] medical,[11] and photonic[12−14] applications. Considerable research work has been done on near-field and far-field coupling effects in nanostructures with many geometries such as nanospheres,[15] nanorods,[16] nanoshells,[17] nanocups,[18] and elliptical nanodisks.[2] When the interparticle distance d is of the order of the wavelength of light and comparable to the isolated nanoparticle resonance wavelength, far-field interaction dominates with d^{-1} dependence.[1] When the interparticle distance is comparable to the nanoparticle size, near-field coupling with d^{-3} dependence dominates.[1,13] This regime can be well modeled by the plasmon hybridization method[19] in complex nanostructures. Many previous studies have shown that the plasmon resonance peak is significantly red-shifted as the interparticle distance is reduced when excited by light with polarization parallel to the interparticle axis. The shift then depends exponentially on the interparticle spacing.[2] Whereas this SPR spectral shift with varying interparticle distance has been extensively studied, thus opening for instance the possibility of measuring very small distances by using a plasmon ruler, the effect on the SPR width has been much less investigated.[20,21] Furthermore, the interparticle distance dependence of the SPR amplitude in nanoparticle arrays has never been quantitatively addressed. Yet, this may be very useful for optimizing plasmonic devices for many applications such as SERS,[22] fluorescence enhancement for biosensing,[23] and absorption enhancement in solar cells.[24] In this paper, the complete plasmon band characteristics of dense spatially ordered 50 nm gold nanoparticle arrays are investigated and quantitatively compared with simulation results. Especially, the

Received: June 26, 2012
Revised: October 30, 2012
Published: October 30, 2012

dx.doi.org/10.1021/jp306292r | J. Phys. Chem. C 2012, 116, 24741−24747

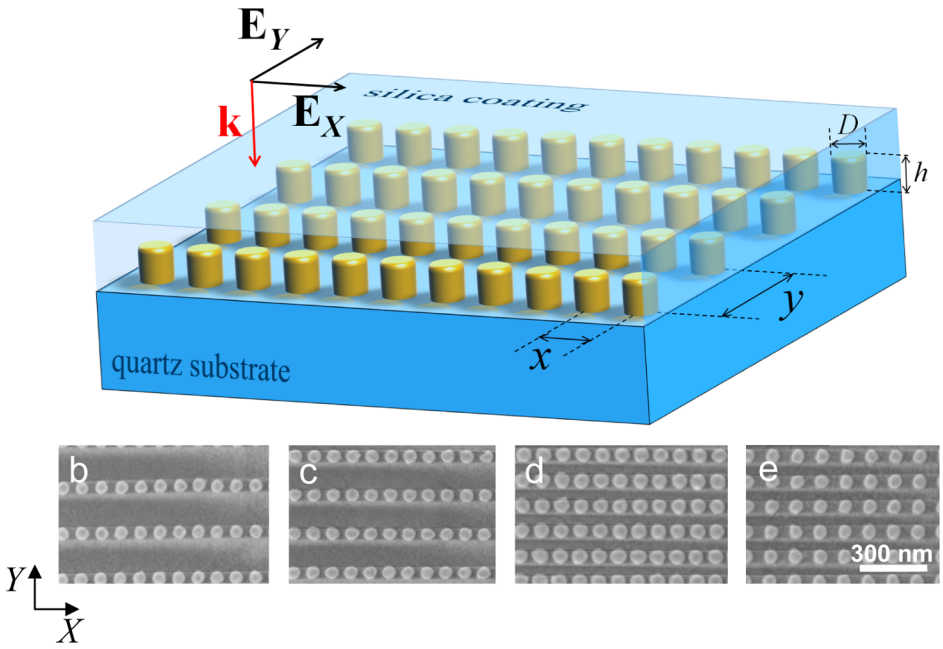

Figure 1. (a) Sketch of the periodic gold nanoparticle arrays. The shape of the particles is a cylinder with $D = h = 50$ nm. The periodicity is x and y in X and Y directions, respectively. (b–d) SEM images of arrays with $x = 80$ nm and $y = 170$, 110, and 80 nm. (e) SEM image of the array with $x = y = 110$ nm.

variation of the SPR wavelength, width, and amplitude with the interparticle distance and polarization direction of the incident light is investigated, pointing out the influence of electrodynamic field phase retardation effects, of the near-field and far-field couplings and of the different plasmon damping mechanisms.

EXPERIMENTAL AND THEORETICAL METHODS

Gold nanoparticles are prepared on a quartz substrate by means of electron beam lithography (VISTEC EBPG 5000 with an accelerating voltage of 100 keV) and lift-off process in PMMA resist. A thin 1 nm Cr layer is deposited before Au deposition in order to strengthen the adhesion between the gold nanoparticles and the quartz substrate. As shown in Figure 1, the nanoparticles are perfectly arranged in periodic arrays with varying periodicity x and y in X and Y directions, respectively. The height h and diameter D are both 50 nm. The edge-to-edge distance between neighboring nanoparticles is tuned down to 30 nm. The different samples are labeled as x–y: 80–170, 80–110, 80–80, and 110–110. All arrays are prepared on the same substrate as 300×300 μm^2 squares, so they can be assumed as two-dimensional (2D) infinitely large at the nanoparticle scale. Scanning electron microscopy (SEM) images of the arrays are shown in Figure 1b–e. The arrays are then protected by the deposition of a 200 nm silica layer by sputtering.

The spectral optical transmission measurements are performed with a homemade setup. The incident monochromatic light is selected with a monochromator (Horiba Jobin–Yvon IHR320) illuminated by a 75 W xenon lamp. The collimated incident light passes a linear polarizer before being slightly focused on the sample at normal incidence with a 50 mm lens. The spot size on the sample has a diameter lower than 150 μm that is sufficiently small to let the whole beam go through the arrays. The propagation and polarization directions are shown in Figure 1a. The transmitted light is collected by another lens and measured with a silicon photodiode over the range 425–800 nm. Transmittance is measured with respect to the substrate. The extinction cross section of one nanoparticle in the array is then deduced from the transmittance spectrum by

$$\sigma_{ext} = -\frac{\ln T}{s}\pi\left(\frac{D}{2}\right)^2 \quad (1)$$

where T is the transmittance obtained from the experiment and s is the surface fraction of gold nanoparticles, that is, the ratio of the surface area occupied by gold in the array and the total area of the array. The peak width (full width at half-maximum) is difficult to measure as the SPR band is asymmetrically distorted by the presence of interband transitions in the same spectral domain as the blue wing of the plasmon band. It is then estimated as twice the difference between the wavelength at half-maximum in the band red wing and the peak maximum wavelength.

We have performed numerical calculations using the discrete dipole approximation (DDA)[25] for the arrays in order to understand our experimental results. The DDA relies on the replacement of the nanoparticle by a large number of dipoles having the polarizability of bulk metal. Each dipole interacts with the external field and the fields scattered by all other dipoles. Thanks to the code DDSCAT 7.1.0 developed by Draine and Flatau,[26] which can solve such periodic targets,[27] we have simulated the extinction, absorption, and scattering efficiencies of a "target unit cell" (one particle) in the infinite arrays, from which the corresponding cross sections can be deduced. For the optical properties of gold nanoparticles, the dielectric function of bulk gold taken from the experimental data of Johnson and Christy[28] has been used, as any size dependence can be neglected for 50 nm particles. For the surrounding dielectric material, dispersion and losses are neglected, and 1.36 is used as the refractive index of silica to account in a phenomenological way for the porosity (about 25% in volume) due to the deposition process.

dx.doi.org/10.1021/jp306292r | J. Phys. Chem. C 2012, 116, 24741–24747

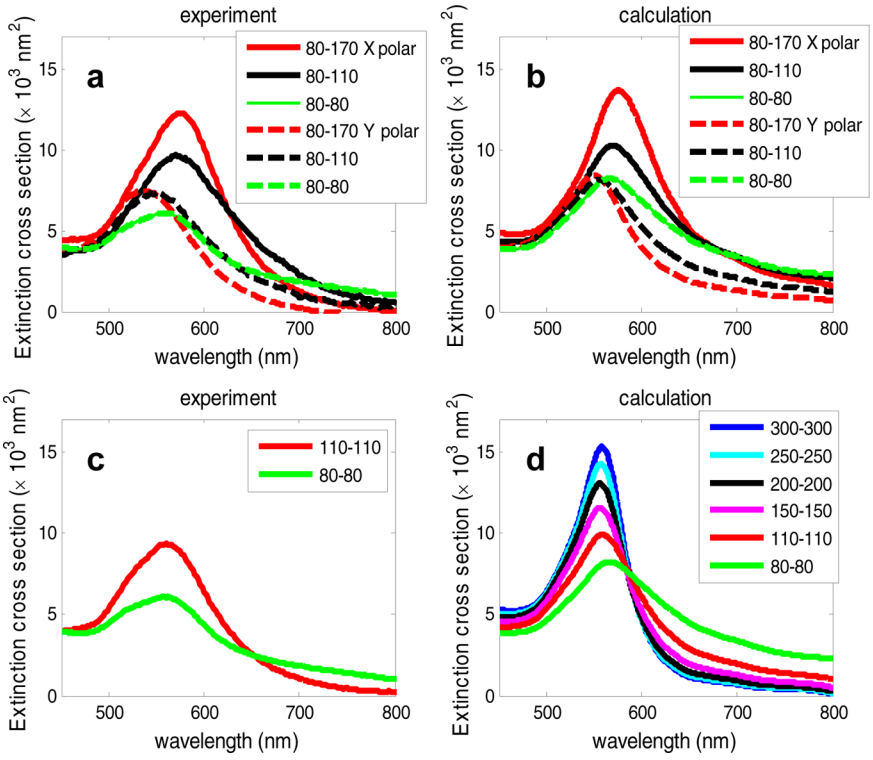

Figure 2. Experimental spectra (a, c) of the extinction cross section of the arrays with different x and y interparticle distances at X and Y field polarizations compared with the calculation results (b, d) obtained by using the DDA. The experimental extinction spectra are determined from the measured transmittance ones. (a, b) Arrays with fixed x = 80 nm and varying y. (c, d) Square arrays with $x = y$. All graphs are displayed at the same scales.

RESULTS AND DISCUSSION

The extinction cross section deduced from the DDA calculations is shown in the right part of Figure 2. Good agreements are observed with the experimental results shown in the left part of Figure 2. The arrays with different periodicity present different plasmon band characteristics. For the arrays with fixed periodicity x shown in Figure 2a and b, the SPR peak blue-shifts, decreases, and broadens with decreasing distance y in X polarization. It red-shifts, slightly decreases, and broadens in Y polarization. Moreover, for the square arrays with $x = y$, as shown in Figure 2c and d, the plasmon resonance decreases and broadens with decreasing periodicity. The calculation additionally predicts a red-shift of the SPR. The slight discrepancies between the experiment and calculation results can be ascribed to the presence of the Cr adhesion layer in the real samples, to the refractive index mismatch between the quartz substrate and the silica coating, and possibly to a slight modification of the porosity of the protective layer related to the density of particles that varies from one array to the other. Moreover, the lift-off process may result in the removal of gold nanoparticles in some zones, leading to the weakening of the mean coupling and the decrease of the real value of the surface density s with respect to its theoretical value, especially for the array with tightly packed nanoparticles (80−80). The width discrepancies can be also explained by the asymmetric band shape that may render our width definition questionable for absorption band profiles as the one of sample 80−80 (see Figure 3). However, the agreement between experimental and calculation results remains good, not only for the SPR wavelength—as it had already been reported in previous studies[3,20,29]—but also for the SPR width and especially amplitude, that is, the absolute value of the nanoparticle extinction cross section that has never been quantitatively addressed in the literature about plasmonic arrays.

To understand the phenomenon more deeply, the optical response of arrays 80−y with fixed x and varying y from 60 to 300 nm has been calculated. This range is chosen because (i) both near-field and far-field couplings occur, which represents an interesting intermediate regime, and (ii) the aim of the present study is to interpret experimental results on arrays with a high density of nanoparticles; the reliability of the elaboration of the latter, in terms of monodispersity of nanoparticle size, shape, and environment, is ensured provided the side-to-side distance between neighboring nanoparticles exceeds a few tens of nanometers. Moreover, additional effects such as electron tunneling across the gap and nonlocal screening of the induced fields would need to be considered at shorter distances, for which the use of classical electrodynamics becomes questionable.[5] This subject, out of the objectives of the present manuscript, has already been investigated, mainly through theoretical works.[30−35]

The evolution of the calculated plasmon band characteristics (peak wavelength, width, and amplitude) with periodicity y is shown in Figure 3 where the experimental results have been added for comparison. In addition, to highlight the phase retardation and far-field radiation (scattering) contributions to the coupling between particles, we have also simulated the plasmon properties of equivalent arrays scaled by $^1/_{10}$ (that is, arrays of particles with $D = h$ = 5 nm, y varying from 6 to 30 nm, and x being fixed at 8 nm) for which the phase retardation and scattering effects can be neglected. Figure 4 shows the plasmon band characteristics as a function of the periodicity y at X and Y polarizations for these small particle arrays. Any

dx.doi.org/10.1021/jp306292r | J. Phys. Chem. C 2012, 116, 24741−24747

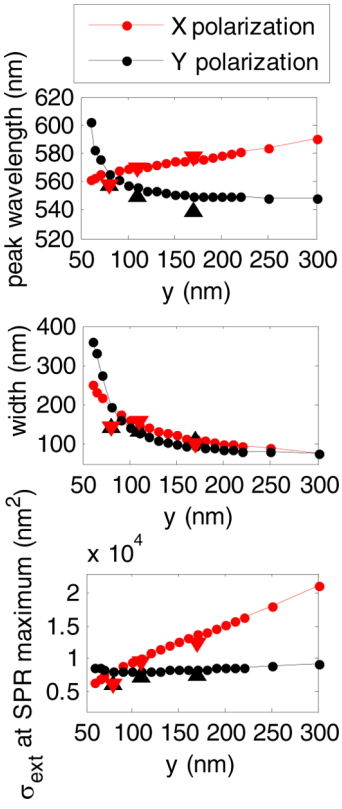

Figure 3. Characteristics of the plasmon band (top: spectral location; middle: width; bottom: amplitude) of 50 nm particle arrays as a function of the periodicity y at X and Y field polarizations, calculated with the DDA method. x is fixed as 80 nm. The triangle symbols are experimental data extracted from Figure 2a for arrays 80−170, 80−110, and 80−80. Red and black colors correspond to X and Y polarizations, respectively.

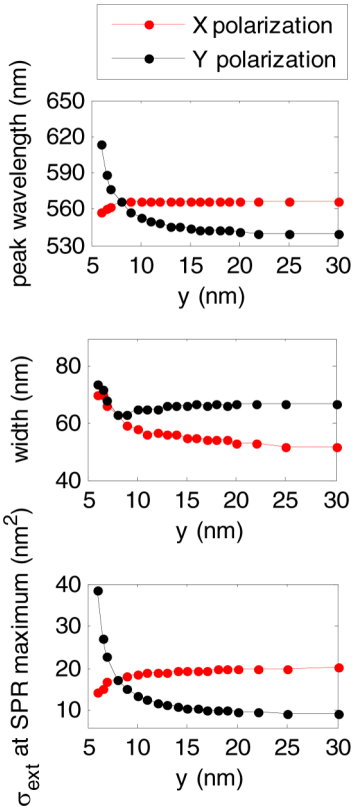

Figure 4. Characteristics of the plasmon band (top: spectral location; middle: width; bottom: amplitude) of 5 nm particle arrays as a function of the periodicity y at X and Y field polarizations, calculated with the DDA method. x is fixed as 8 nm. Red and black colors correspond to X and Y polarizations, respectively.

quantum confinement effect leading to the size dependence of the dielectric function is disregarded here. For all arrays with the same periodicity x, the variations with distance y of the SPR characteristics can be ascribed to the variation of the coupling between particle chains. We will then especially focus on the variation with y of the coupling in the Y direction in the following discussion. As can be observed in Figures 3 and 4, the SPR peak wavelength, width, and amplitude display a partially different variation with periodicity y at both polarizations.

For small particle arrays, the coupling occurs mainly in the near field rather than in the far field: in the long distance range (from 20 to 30 nm on Figure 4), there is nearly no variation of the plasmon band characteristics. The small particle arrays can be qualitatively described by the electrostatic dipolar interaction,[36] from which the following can be deduced: (i) in Y polarization, the field induced in one particle by the rest of the particles has the same direction as the applied field and adds constructively, weakening the inner restoring force in each particle, and consequently, a red-shift and an enhancement of the SPR are induced when increasing this coupling (i.e., when decreasing y); (ii) in X polarization, the induced local field between two nanoparticles in the Y direction opposes the applied field, thus reinforcing the restoring force, and a slight blue-shift and a weak damping of the SPR are thereby observed with decreasing y. The topography, in the median plane of the nanoparticles, of the field enhancement (that is, the ratio of the amplitudes of the local and applied fields) and the field phase (that is, the phase difference between the local and applied fields) has been calculated by using the DDA. These distributions are displayed in Figure 5 for the array 8−11 in X and Y polarizations. From Figure 5c and d, it can be deduced that the phase of the induced near field between two nanoparticles in the Y direction is larger (respectively lower) than 90° in X (respectively Y) polarization, which means that the induced field adds to the applied field destructively

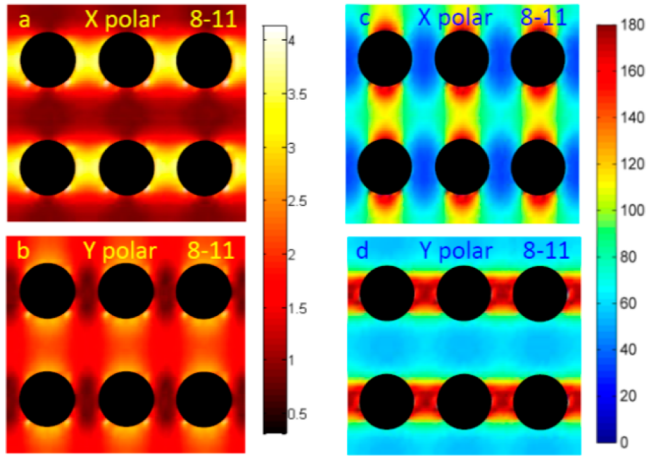

Figure 5. Distribution of the field amplitude enhancement (a, b) and field phase (c, d) in the array 8−11. (a, c) are for X field polarization, and (b, d) are for Y polarization.

dx.doi.org/10.1021/jp306292r | J. Phys. Chem. C 2012, 116, 24741−24747

(respectively constructively). These numerical results are consistent with the expectation of the electrostatic approximation. As shown in Figure 5a and b, the induced near field dominates in the direction parallel to the induced dipole axis[36] (then for *Y* polarization in the case of coupling in the *Y* direction). This explains why the red-shift of the SPR following the decrease of *y* in *Y* polarization is more significant than the blue-shift in *X* polarization, as displayed in Figure 4.

For large particle arrays, both near-field and far-field coupling need to be considered. The field enhancement and phase distributions in three large particle arrays (80−60, 80−110, and 80−250) in *X* and *Y* polarizations are shown in Figures 6 and 7,

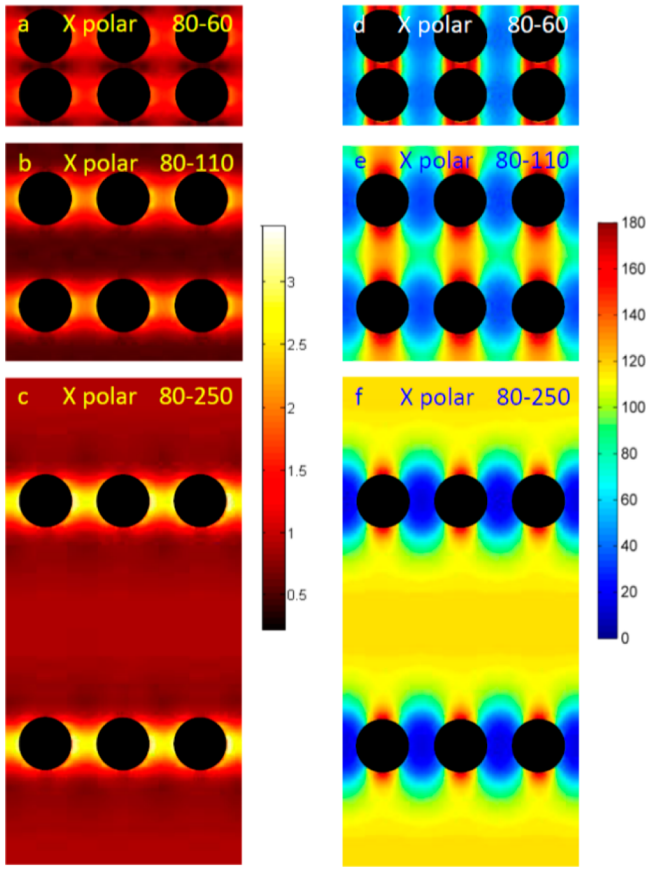

Figure 6. Distribution of the field amplitude enhancement (a−c) and field phase (d−f) in *X* polarization for arrays 80−60, 80−110, and 80−250.

respectively. The color map scale is kept the same for sake of easy comparison. Far-field radiation dominates in the direction perpendicular to the applied field. Consequently, for *X* polarization and long *y* distances, the coupling in the *Y* direction is mainly ensured by far-field radiation. On the contrary, in *Y* polarization, the far-field interaction between nanoparticles in the *Y* direction is very weak. From the phase distribution in the array 80−250 in *X* polarization, shown in Figure 6f, it can be deduced that the induced far field adds to the applied field destructively between two nanoparticle chains. In *Y* polarization, the near-field coupling only works efficiently, which adds to the applied field constructively. This explains the blue-shift and the red-shift of the SPR when decreasing *y* in *X* and *Y* polarizations, respectively (see Figure 3). Moreover, due to the respective spatial extension ranges of the near-field and far-field radiations, the magnitude of the blue-shift in *X*

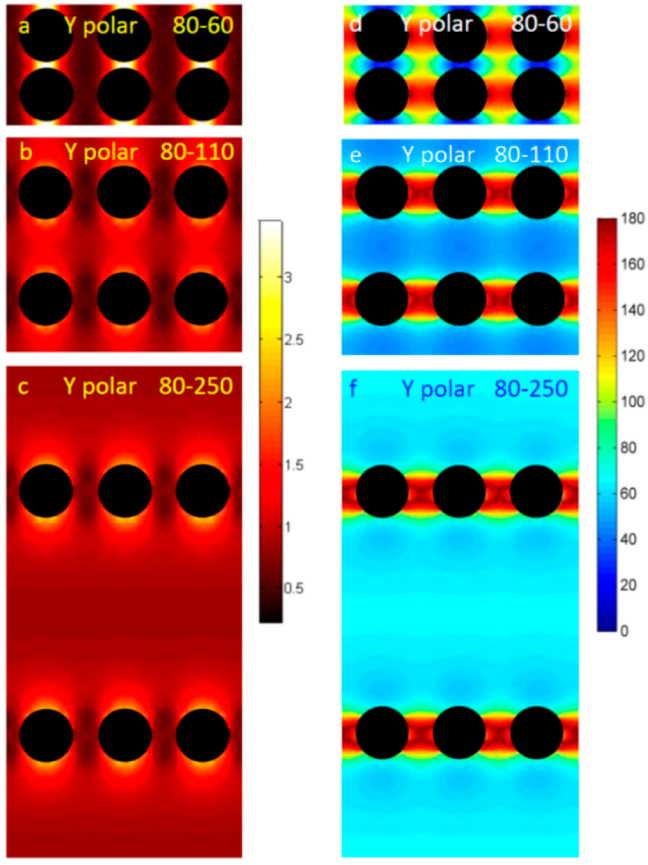

Figure 7. Distribution of the field amplitude enhancement (a−c) and field phase (d−f) in *Y* polarization for arrays 80−60, 80−110, and 80−250.

polarization is larger than the one of the red-shift in *Y* polarization when *y* is reduced from 300 to 200 nm; then from *y* = 200 to 60 nm, the blue-shift is weaker than the red shift. This also explains the initial blue-shift and then the red-shift with decreasing periodicity in the square arrays with *x* = *y*, as shown in Figure 2d.

For arrays of identical nanoparticles, the spectral width of the plasmon resonance is directly related to its decay time. The decay time is determined by the damping of the plasmon oscillation, which has been discussed in the literature for single particles such as nanospheres,[37] nanorods,[38] and nanoprisms.[39] Two kinds of damping are involved:[21,38−40] radiative damping (scattering), which results from the reradiation of the incoming electromagnetic wave, and nonradiative damping, that is, energetic relaxation (absorption) mainly due to electron−electron and electron−phonon collisions. As the size of the particles is kept constant for all arrays, the electron surface scattering[38] does not affect the SPR width evolution with varying *x* and *y* periodicities and will then not be considered here. Previous works have shown that radiation damping broadens the SPR band.[38,39] Consequently, higher electromagnetic scattering results in larger damping and then a broader SPR band. On the contrary, a higher fraction of absorption in extinction, that is, a lower fraction of scattering and then a lower radiative damping, goes together with a narrower SPR band. So, the width of the plasmon band of the arrays is determined by competing absorption and scattering processes. If an increase of extinction and a decrease of width are observed together when varying *y*, then the variation of

dx.doi.org/10.1021/jp306292r | J. Phys. Chem. C 2012, 116, 24741−24747

absorption losses dominates over the variation of scattering ones. As shown in Figure 3, in X polarization, the extinction amplitude decreases and the width increases with decreasing y; that means the y dependence of the damping is dominated by the variation of the nonradiative contribution in this case. In Y polarization, the extinction cross section at SPR first slightly decreases with decreasing y in the long distance range and then increases at shorter distances. Meanwhile, the width increases over the whole distance range when decreasing y. Thus, in Y polarization, the contribution of the nonradiative damping variation with y dominates in the long distance range while the radiative damping contribution dominates at closer distances. Let us now point out that both the near-field and far-field couplings between nanoparticles contribute to the radiative losses. Consequently, if there is a strong variation of the far-field coupling (which is the case of X polarization at long distances), then the variation of the radiative damping with y has a greater contribution in X polarization than in Y polarization. Similarly, a strong variation of the near-field coupling (case of Y polarization at short distances) implies that the variation of the radiative damping has a greater contribution in Y polarization than in X polarization. These results, obtained with the DDA numerical approach, have been confirmed by carrying out the semianalytical model based on the retarded dipole sum initially proposed by Markel[41] and then by Schatz and co-workers[20] for infinite periodic chains and arrays. In this approach, the retarded dipole sum, S, consists of electrostatic ($\sim 1/r^3$), radiative ($\sim 1/r$), and retardation ($\sim e^{i\mathbf{k}\cdot\mathbf{r}}$) contributions, where $\mathbf{k}$ and $\mathbf{r}$ (of norm r) denote the wave and coordinate vectors, respectively. The real part of S then determines the plasmon resonance wavelength while its imaginary part determines the plasmon bandwidth.

It is finally worth comparing the plasmon band characteristics of the 5 nm and 50 nm nanoparticle arrays shown in Figures 3 and 4. As stated above, for both kinds of arrays, the interaction between chains in Y polarization occurs mainly through near-field coupling—with a negligible radiative damping contribution—the spatial extension of which is very limited. This explains the quasi-constant values of the SPR characteristics in the long distance range (200−300 nm in Figure 3 and 20−30 nm in Figure 4). The reasons for which very weak variations are nevertheless observed in 50 nm nanoparticle arrays may include (i) the residual far-field coupling stemming from the fact that the nanoparticles are not perfect pointlike dipoles and (ii) the additional phase retardation contribution. In X polarization, both near-field and far-field couplings work in 50 nm particle arrays, while the near-field coupling only is involved in small particle arrays. The effect of the far-field coupling in the long distance range can be evidently seen in Figure 3. Let us now focus on the damping mechanisms. In the distance range from 80 to 300 nm for large arrays and 8 to 30 nm for small ones, the SPR peak width and amplitude exhibit according trends: the peak broadening (narrowing) corresponds to the decrease (increase) of its amplitude. As explained earlier, this means that the contribution of the intrinsic absorption damping mechanism to the dependence of the SPR characteristics on the interparticle distance dominates in both kinds of arrays within this range, although the radiative losses can be comparable or even larger than the nonradiative ones in 50 nm particle arrays, contrary to 5 nm arrays where scattering is negligible. At shorter distances, the radiative damping variation with y dominates in Y polarization for both kinds of arrays due to the near-field coupling effect.

CONCLUSIONS

In summary, we have studied experimentally and theoretically the interparticle coupling effects on the plasmon band characteristics in dense and ordered 2D arrays of 50 nm gold nanoparticles with varying periodicity. Blue-shift, damping, and broadening of the plasmon resonance are induced by decreasing the periodicity in the direction perpendicular to the polarization, while decreasing the periodicity in the direction parallel to the polarization results in the SPR red-shift, first damping, then enhancing, and broadening. For the arrays with fixed x periodicity, the SPR peak wavelength, width, and amplitude display monotonic evolution with varying y periodicity. For the square arrays with the same x and y, the resonance decreases and broadens but the peak wavelength blue-shifts first and then red-shifts with decreasing the periodicity from 300 to 80 nm. The phenomenon has been examined and explained by using numerical calculations based on the DDA as well as the simple semianalytical model based on the coupled dipole approximation. The retardation and interparticle radiative coupling effects result in decreasing amplitude and broadening of the plasmon band under longitudinal polarization. In order to highlight these effects, we have simulated the equivalent arrays scaled by $^1/_{10}$ the optical response of which can be well described by electrostatic dipolar interactions. The plasmon band characteristics exhibit partially different trends from the ones of 50 nm particle arrays. In addition, for the arrays with large y periodicity, the contribution of the energetic relaxation damping mechanism to the y dependence of the SPR characteristics dominates over the one of radiation damping. In the shorter distance range, the radiative damping variation with y dominates in the longitudinal polarization due to the near-field coupling effect. Beyond their interest for understanding more deeply the role of electromagnetic couplings in the optical response of ensembles of metal nanoparticles, these results may be useful for the design and optimization of plasmonic devices for chemical and biological sensing as well as for improving the yield of photovoltaic cells.

AUTHOR INFORMATION

Corresponding Author

*Phone: +33-141131626; e-mail: bruno.palpant@ecp.fr.

Notes

The authors declare no competing financial interest.

ACKNOWLEDGMENTS

X.W. wants to thank China Scholarship Council for the financial support.

REFERENCES

(1) Halas, N. J.; Lal, S.; Chang, W.-S.; Link, S.; Nordlander, P. *Chem. Rev.* **2011**, *111*, 3913−3961.
(2) Su, K.-H.; Wei, Q.-H.; Zhang, X. *Nano Lett.* **2003**, *3*, 1087−1090.
(3) Wei, Q.-H.; Su, K.-H.; Durant, S.; Zhang, X. *Nano Lett.* **2004**, *4*, 1067−1071.
(4) Jain, P. K.; El-Sayed, M. A. *Chem. Phys. Lett.* **2010**, *487*, 153−164.
(5) Hao, E.; Schatz, G. C. *J. Chem. Phys.* **2004**, *120*, 357−366.
(6) Nie, S.; Steven, R. E. *Science* **1997**, *275*, 1102−1106.
(7) Nikoobakht, B.; Wang, J.; El-Sayed, M. A. *Chem. Phys. Lett.* **2002**, *366*, 17−23.
(8) Kneipp, K.; Wang, Y.; Kneipp, H.; Perelman, L. T.; Itzkan, I.; Dasari, R. R.; Feld, M. S. *Phys. Rev. Lett.* **1997**, *78*, 1667−1670.

(9) Elghanian, R.; Storhoff, J. J.; Mucic, R. C.; Letsinger, R. L.; Mirkin, C. A. *Science* **1997**, *277*, 1078−1081.
(10) Willets, K. A.; Van Duyne, R. P. *Annu. Rev. Phys. Chem.* **2007**, *58*, 267−297.
(11) Kim, D.; Jeong, Y.; Jon, S. *ACS Nano* **2010**, *4*, 3689−3696.
(12) Inouye, H.; Tanaka, K. *Jpn. J. Appl. Phys.* **2000**, *39*, 5132−5133.
(13) Maier, S.; Brongersma, M.; Kik, P.; Atwater, H. *Phys. Rev. B* **2002**, *65*, 193408.
(14) Bouchon, P.; Koechlin, C.; Pardo, F.; Pelouard, J.-L.; Haidar, R. *Opt. Lett.* **2012**, *37*, 1038−1040.
(15) Ezequiel, R. E.; Eduardo, A. C. *J. Phys. Chem. C* **2010**, *114*, 3918−3923.
(16) Jain, P. K.; Eustis, S.; El-Sayed, M. A. *J. Phys. Chem. B* **2006**, *110*, 18243−18253.
(17) Bardhan, R.; Grady, N. K.; Ali, T.; Halas, N. J. *ACS Nano* **2010**, *4*, 6169−6179.
(18) King, N. S.; Li, Y.; Ayala-Orozco, C.; Brannan, T.; Nordlander, P.; Halas, N. J. *ACS Nano* **2011**, *5*, 7254−7262.
(19) Prodan, E. *Science* **2003**, *302*, 419−422.
(20) Zhao, L. L.; Kelly, K. L.; Schatz, G. C. *J. Phys. Chem. B* **2003**, *107*, 7343−7350.
(21) Zoric, I.; Zach, M.; Kasemo, B.; Langhammer, C. *ACS Nano* **2011**, *5*, 2535−2546.
(22) Yan, B.; Boriskina, S. V.; Reinhard, B. M. *J. Phys. Chem. C* **2011**, *115*, 24437−24453.
(23) Corrigan, T. D.; Guo, S. H.; Szmacinski, H.; Phaneuf, R. J. *Appl. Phys. Lett.* **2006**, *88*, 101112.
(24) Rockstuhl, C.; Lederer, F. *Appl. Phys. Lett.* **2009**, *94*, 213102.
(25) Draine, B. T. *Astrophys. J.* **1988**, *333*, 848−872.
(26) Draine, B. T.; Flatau, P. J. *User Guide for the Discrete Dipole Approximation Code DDSCAT 7.1*; 2010; http://arxiv.org/abs/1002.1505.
(27) Draine, B. T.; Flatau, P. J. *J. Opt. Soc. Am. A* **2008**, *25*, 2693−2703.
(28) Johnson, P. B.; Christy, R. W. *Phys. Rev. B* **1972**, *6*, 4370−4379.
(29) Lamprecht, B.; Schider, G.; Lechner, R. T.; Ditlbacher, H.; Krenn, J. R.; Leitner, A.; Aussenegg, F. R. *Phys. Rev. Lett.* **2000**, *84*, 4721−4724.
(30) Rechberger, W.; Hohenau, A.; Leitner, A.; Krenn, J. R.; Lamprecht, B.; Aussenegg, F. R. *Opt. Commun.* **2003**, *220*, 137−141.
(31) Romero, I.; Aizpurua, J.; Bryant, G. W.; García de Abajo, F. J. *Opt. Express* **2006**, *14*, 9988−9999.
(32) Jain, P. K.; Huang, W.; El-Sayed, M. A. *Nano Lett.* **2007**, *7*, 2080−2088.
(33) Klimov, V. V.; Guzatov, D. V. *Appl. Phys. A: Mater. Sci. Process.* **2007**, *89*, 305−314.
(34) García de Abajo, F. J. *J. Phys. Chem. C* **2008**, *112*, 17983−17987.
(35) Zabkov, I.; Klimov, V. V.; Treshin, I.; Glazov, O. *Quantum Electron.* **2011**, *41*, 742−747.
(36) Pinchuk, A.; Schatz, G. *Mater. Sci. Eng., B* **2008**, *149*, 251−258.
(37) Klar, T.; Perner, M.; Grosse, S.; von Plessen, G.; Spirkl, W.; Feldmann, J. *Phys. Rev. Lett.* **1998**, *80*, 4249−4252.
(38) Novo, C.; Gomez, D.; Perez-Juste, J.; Zhang, Z.; Petrova, H.; Reismann, M.; Mulvaney, P.; Hartland, G. V. *Phys. Chem. Chem. Phys.* **2006**, *8*, 3540−3546.
(39) Blaber, M. G.; Henry, A.-I.; Bingham, J. M.; Schatz, G. C.; Van Duyne, R. P. *J. Phys. Chem. C* **2012**, *116*, 393−403.
(40) Hohenau, A.; Leitner, A.; Aussenegg, F. R. Near-field and far-field properties of nanoparticle arrays. In *Surface Plasmon Nanophotonics*; Brongersma, M. L., Kik, P. G., Eds.; Springer: Dordrecht, The Netherlands, 2007; pp 14−15.
(41) Markel, V. A. *J. Mod. Opt.* **1993**, *40*, 2281−2291.